

Prescription for the fraction of delocalized eigenstates in the long-range AAH model

Nilanjan Roy and Auditya Sharma

Department of Physics, Indian Institute of Science Education and Research, Bhopal, Madhya Pradesh 462066, India

(Dated: December 5, 2021)

We uncover a systematic structure in the single particle phase-diagram of the quasi-periodic Aubry-André-Harper(AAH) model with power-law hoppings ($\sim \frac{1}{r^\sigma}$) when the quasi-periodicity parameter is chosen to be a member of the ‘metallic mean family’ of irrational Diophantine numbers. In addition to the fully delocalized and localized phases we find a co-existence of multifractal (localized) states with the delocalized states for $\sigma < 1$ ($\sigma > 1$). The fraction of delocalized eigenstates in these phases can be obtained from a general sequence, which is a manifestation of a mathematical property of the ‘metallic mean family’. The entanglement entropy of the noninteracting many-body ground states respects the area-law if the Fermi level belongs in the localized regime while logarithmically violating it if the Fermi-level belongs in the delocalized or multifractal regimes. Entanglement entropy shows the area-law even in the delocalized regime for special filling fractions, which are related to the metallic means.

Quasi-periodic systems exhibit non-trivial localization properties [1–4] despite the simplicity of the models involved. Unlike a random potential as in the Anderson model [5], a quasi-periodic potential as in the Aubry-André-Harper(AAH) model shows a delocalization-localization transition at a non-zero finite strength of the potential even in one dimension [6, 7]. Even the co-existence of delocalized and localized eigenstates (mobility edge as in the Anderson model in three dimensions) has been reported in some variants of the AAH model [8, 9] in one dimension. The AAH potential has been realized in the experiments of ultracold atoms studying single particle localization [10–12] and ‘many body localization’ [13], which has led to a fresh wave of interest [14–16] in interacting quasi-periodic systems [17–20]. There have also been many finite temperature studies of the model [21–23] in recent times.

The study of Hamiltonians with power-law hoppings or interactions ($\propto \frac{1}{r^\sigma}$) has seen a resurgence of interest after such Hamiltonians were realized in experiments of ultra-cold systems [24–37]. When the hopping strength is sufficiently long-ranged, instead of the exponentially localized eigenstates seen in short-range models, one obtains algebraically localized eigenstates. In the power-law random hopping model in one dimension algebraic localization is found for $\sigma > 1$ [38, 39] whereas power-law hoppings coupled with random onsite disorder can show algebraic localization for all values of σ [40, 41]. The effect of power-law hoppings on the quasi-periodic AAH potential has also been studied very recently [42]. The study has uncovered the systematic appearance of multifractal (localized) eigenstates which co-exist with delocalized eigenstates for $\sigma < 1$ ($\sigma > 1$) [42]. The irrationality of the quasiperiodicity parameter (α) is what renders the Hamiltonian quasiperiodic. The fraction of delocalized eigenstates in the different phases of the system is related to the precise value of α , which is usually set to be the ‘golden mean’ $(\sqrt{5} - 1)/2$. The ‘golden mean’ is a member of a broader class called the ‘metal-

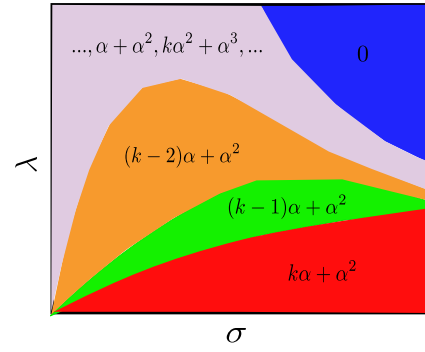


FIG. 1. Schematic of the phases of a single particle in the LRH model for the quasi-periodicity parameter α , shown in different colors. The colored phases are also labelled by the fraction of delocalized eigenstates (η) as shown in the figure. Here $k = 1, 2, 3$ when α is ‘golden mean’, ‘silver mean’ and ‘bronze mean’ respectively. The strength of the quasi-periodic potential and power-law hopping parameter are denoted as λ and σ respectively.

lic mean family’, which is a set of irrational Diophantine numbers and will be discussed in more detail ahead.

In this Letter, we chart out the phase diagram of a single particle in the presence of the AAH potential and power-law hoppings when α is set to be a member of the ‘metallic mean family’, with special attention given to the ‘golden mean’, ‘silver mean’ and ‘bronze mean’. In addition to the delocalized and localized phases, we obtain mixed phases where the multifractal (localized) states can co-exist with delocalized states for $\sigma < 1$ ($\sigma > 1$). One of the key findings of our work is that the fraction of delocalized eigenstates in these phases can be obtained from a general sequence, which is related to a mathematical property of the metallic means (see schematic in Fig. 1). Moreover we calculate the entanglement entropy, an extensively used quantity to study localization phenomena [43, 44], of the noninteracting fermionic many-body ground states to characterize different phases in the model. In the delocalized regime entanglement entropy is surprisingly found to follow the area-law for the special

filling fractions which are related to the metallic means. Such behavior for special filling fractions is also found in the well known nearest neighbor hopping limit [45].

LRH model: The model of interest is the one dimensional long-range AAH (LRH) model given by the Hamiltonian:

$$H = - \sum_{i < j}^N \left(\frac{J}{r_{ij}^\sigma} \hat{c}_i^\dagger \hat{c}_j + H.c. \right) + \lambda \sum_{i=1}^N \cos(2\pi\alpha i + \theta_p) \hat{n}_i, \quad (1)$$

where \hat{c}_i^\dagger (\hat{c}_i) represents the single particle creation (destruction) operator at site i and corresponding number operator $\hat{n}_i = \hat{c}_i^\dagger \hat{c}_i$. We consider a lattice of total number of sites N , where r_{ij} is the geometric distance between the sites i and j in a ring. Here λ is the strength of the quasi-periodic potential with the parameter α chosen to be a Diophantine irrational number [46] e.g. $(\sqrt{5}-1)/2$. θ_p is an arbitrary global phase. The strength of the long range hopping is controlled by J and the long range parameter in the hopping σ . We will assume $J = 1$ for all the numerics. In the $\sigma \rightarrow \infty$ limit this model becomes the celebrated Aubry-André-Harper (AAH) model [6, 7]. As a consequence of self-duality [6, 7], all the eigenstates are delocalized for $\lambda < 2J$ and localized for $\lambda > 2J$ [46] (see Ref. 47). For a finite σ self-duality is broken.

Metallic mean family: Any irrational number can be written as a continued fraction [48] which allows for a successive rational approximation of it in the form of a/b where a, b are co-prime numbers. For Diophantine numbers there always exists a lower bound to how closely such irrational numbers may be represented by rational approximations, such that $|\alpha - \frac{a}{b}| > \epsilon/b^{2+\zeta}$ with $\epsilon > 0$ and $\zeta \geq 0$ [49, 50]. The above property is a sign of the strength of the irrationality of Diophantine numbers.

It is useful to consider a generalized ‘ k -Fibonacci sequence’ [51], given by

$$F_u = kF_{u-1} + F_{u-2}, \quad (2)$$

with $F_0 = 0, F_1 = 1$. The limit $\alpha = \lim_{u \rightarrow \infty} F_{u-1}/F_u$ with $k = 1, 2, 3, \dots$ yields the ‘metallic mean family’, the first three members of which are the well-known ‘golden mean’ ($\alpha_g = (\sqrt{5}-1)/2$), the ‘silver mean’ ($\alpha_s = \sqrt{2}-1$) and ‘bronze mean’ ($\alpha_b = (\sqrt{13}-3)/2$) respectively. A slowly converging sequence of rational approximations of these Diophantine numbers is given by F_{u-1}/F_u for two successive members in the sequence for a fixed integer k . Each member α of the ‘metallic mean’ family satisfies the following relation:

$$(\alpha)^z = k(\alpha)^{z+1} + (\alpha)^{z+2}, \quad (3)$$

where $k = 1, 2, 3, \dots$ for $\alpha = \alpha_g, \alpha_s, \alpha_b, \dots$ respectively, and z is a non-negative integer. Putting $z = 0$ in Eq. 3 also yields an important case namely, $k\alpha + \alpha^2 = 1$.

Phase diagram: Now we consider a single particle in the LRH model with different parameters α_g, α_s and α_b

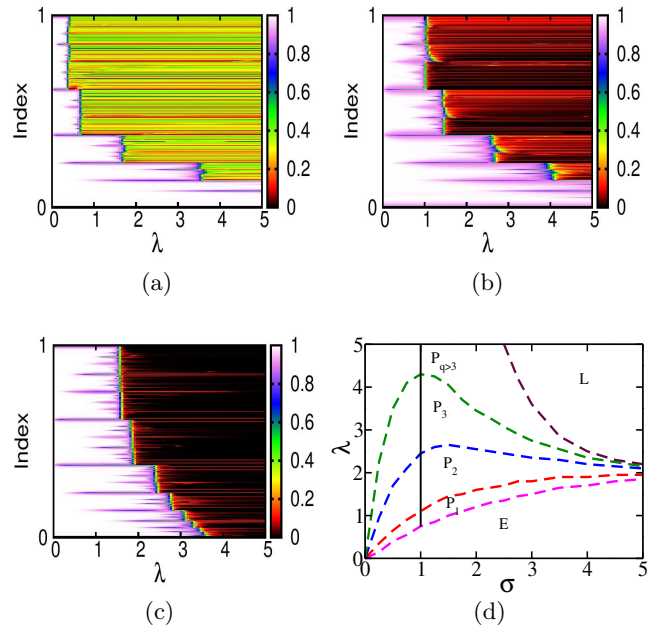


FIG. 2. (a-c) Fractal dimension D_2 (in color) as a function of λ and increasing fractional eigenstate index n/N starting from the ground state for α_g and $\sigma = 0.5, 1.5$ and 3.0 respectively. For all the plots, $N = 1000$ and $\delta = 0.02$. (d) Phase diagram: in addition to extended (E) and localized (L) phases with $\eta = 1, 0$ respectively, the mixed phases P_1, P_2, P_3, \dots exist with $\eta = \alpha_g, \alpha_g^2, \alpha_g^3, \dots$. The vertical line separates out the DM edge for $\sigma < 1$ from the DL edge for $\sigma > 1$.

which are members of the ‘metallic mean family’. In order to determine the phases we calculate the fractal dimension of the eigenstates for $\theta_p = 0$. We employ the box counting procedure to determine the fractal dimension [52–55]. Dividing the system of N sites into $N_l = N/l$ boxes of l sites each, the ‘fractal dimension’ is defined as:

$$D_f = \lim_{\delta \rightarrow 0} \frac{1}{f-1} \frac{\ln \sum_{m=1}^{N_l} (\mathcal{I}_m)^f}{\ln \delta}, \quad (4)$$

where $\mathcal{I}_m = \sum_{i \in m} |\psi_n(i)|^2$ computed inside the m^{th} box for the n^{th} eigenstate $|\psi_n\rangle$ and $\delta = 1/N_l$. In the perfectly delocalized (localized) phase D_f is unity (zero), whereas for a multifractal state D_f shows a non-trivial dependence on f and $0 < D_f < 1$.

Fig. 2(a-c) shows D_2 as a function of λ for all the single particle eigenstates when the quasiperiodicity parameter is fixed at α_g for $\sigma = 0.5, 1.5$ and 3.0 respectively. As can be seen from Fig. 2(a) for $\sigma = 0.5$, the fraction of delocalized eigenstates decreases and fractal states ($0 < D_2 < 1$) appear in blocks as λ increases. We have also checked that in fact D_f depends on f for these blocks of states, which is a signature of multifractality (see Ref. 47). Hence there exists a delocalized-to-multifractal (DM) edge in the eigenstate spectrum. The DM edge goes down in steps as the fraction of delocalized eigenstates decreases with λ . However, the position

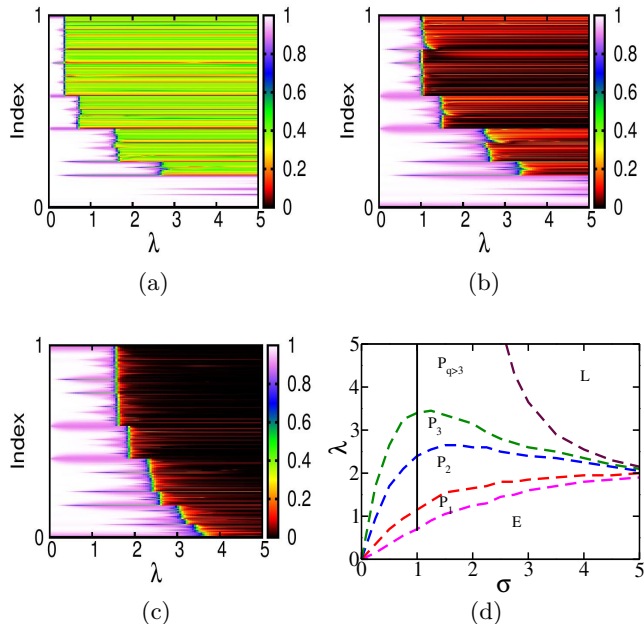


FIG. 3. (a-c) Fractal dimension D_2 (in color) as a function of λ and increasing fractional eigenstate index n/N starting from the ground state for α_s and $\sigma = 0.5, 1.5$ and 3.0 respectively. For all the plots, $N = 1000$ and $\delta = 0.02$. (d) Phase diagram: in addition to extended (E) and localized (L) phases with $\eta = 1, 0$ respectively, the mixed phases P_1, P_2, P_3, \dots exist with $\eta = \alpha_s + \alpha_s^2, \alpha_s, \alpha_s^2 + \alpha_s^3, \dots$. The vertical line separates out the DM edge for $\sigma < 1$ from the DL edge for $\sigma > 1$.

of the DM edge remains unchanged within each step as the fraction of delocalized eigenstates (denoted as η hereafter) stays constant in that region. It is found that in the decreasing step-like regions defined by constant DM edges, $\eta = \alpha_g, \alpha_g^2, \alpha_g^3, \dots$. We denote the step-like regions as P_q ($q = 1, 2, 3, \dots$) phases with $\eta = \alpha_g, \alpha_g^2, \alpha_g^3, \dots$ respectively.

Fig. 2(b,c) for $\sigma = 1.5$ and 3.0 respectively show the appearance of blocks of localized states ($D_2 \approx 0$) with increasing λ . This implies that there exists a delocalized-to-localized (DL) edge, also well known as the mobility edge. Similar to DM edges these fixed DL-edge containing phases are also denoted as P_q ($q = 1, 2, 3, \dots$) for $\eta = \alpha_g, \alpha_g^2, \alpha_g^3, \dots$ respectively. D_2 of all the eigenstates for α_s and increasing λ is shown in Fig. 3(a-c) for $\sigma = 0.5, 1.5, 3.0$ respectively. For α_s one obtains P_1, P_2, P_3, \dots phases with $\eta = \alpha_s + \alpha_s^2, \alpha_s, \alpha_s^2 + \alpha_s^3, \dots$ and DM edges (for $\sigma = 0.5$) and DL edges (for $\sigma = 1.5, 3.0$). Similarly from Fig. 4(a-c) for α_b and $\sigma = 0.5, 1.5, 3.0$ respectively one obtains P_1, P_2, P_3, \dots phases with $\eta = 2\alpha_b + \alpha_b^2, \alpha_b + \alpha_b^2, \alpha_b, \dots$ and DM edges (for $\sigma = 0.5$) and DL edges (for $\sigma = 1.5, 3.0$).

After an extensive analysis, we find that in a particular P_q phase, the same blocks of multifractal states become localized as one crosses $\sigma = 1$ whereas the corresponding η remains the same. We chart out the single-particle phase diagram for the parameter α_g in Fig 2(d), which is

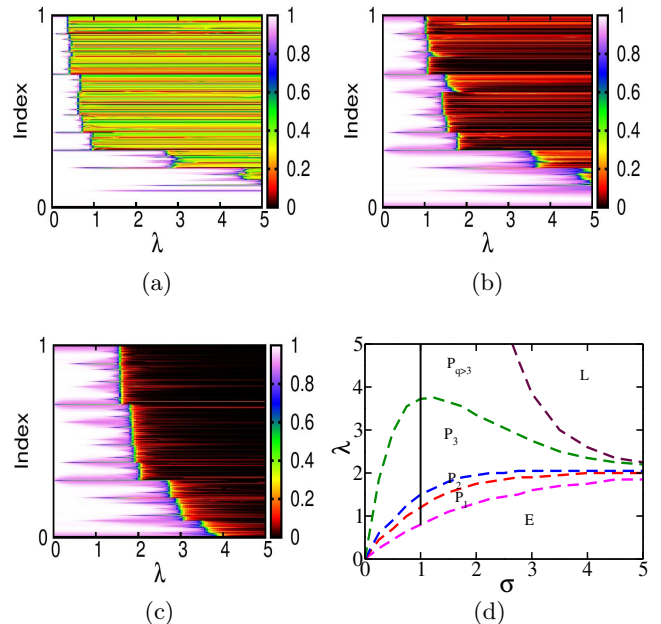


FIG. 4. (a-c) Fractal dimension D_2 (in color) as a function of λ and increasing fractional eigenstate index n/N starting from the ground state for α_b and $\sigma = 0.5, 1.5$ and 3.0 respectively. For all the plots, $N = 1000$ and $\delta = 0.02$. (d) Phase diagram: in addition to extended (E) and localized (L) phases with $\eta = 1, 0$ respectively, the mixed phases P_1, P_2, P_3, \dots exist with $\eta = 2\alpha_b + \alpha_b^2, \alpha_b + \alpha_b^2, \alpha_b, \dots$. The vertical line separates out the DM edge for $\sigma < 1$ from the DL edge for $\sigma > 1$.

also obtained in Ref. 42 for a Fibonacci N . Fig 2(d) contains weakly multifractal eigenstates, similar to the AAH model (see Ref. 47), even in the delocalized regimes due to the choice of a non-Fibonacci N . It is to be noted that as σ increases the extent of the mixed phases shrinks as the LRH model approaches the AAH limit. The phase diagrams for α_s and α_b are shown in Fig. 3(d) and Fig. 4(d) respectively. The P_q phases (corresponding to α_s and α_b) in these cases as well, like with α_g , contain DM edges for $\sigma < 1$ and DL edges for $\sigma > 1$. The changes in P_q phases at $\sigma = 1$ are denoted by the vertical lines in all the phase diagrams.

Fraction of delocalized states: After a careful observation of the phase diagrams, one may propose a sequence which dictates the values of η in P_q phases corresponding to different quasi-periodicity parameters α , which belong to the ‘metallic mean family’ described in Eq. 2. For any $\sigma > 0$ without disorder ($\lambda = 0$), $\eta = k\alpha + \alpha^2 = 1$ where $k = 1, 2, 3$ correspond to $\alpha_g, \alpha_s, \alpha_b$ respectively and $z = 0$ in Eq. 3. As the quasi-periodic disorder is turned on ($\lambda \neq 0$), η starts decreasing in a sequence according to Eq. 3 for the ‘metallic mean family’, which is depicted in Fig. 5. Eq. 3 implies that one can always express $(\alpha)^z$ as a sum of two bits $k(\alpha)^{z+1}$ and $(\alpha)^{z+2}$. In the LRH model the bigger bit loses weight at every step becoming $(k-1)\alpha^{z+1}, (k-2)\alpha^{z+1}, \dots$ until it reaches α^{z+1} , where it disintegrates again according to the rule defined

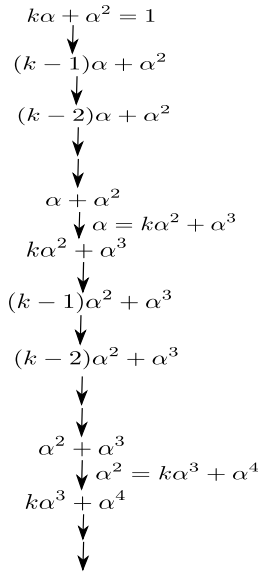


FIG. 5. Depicts how the fraction of delocalized eigenstates (η) decreases in a manner that uses the rule defined in Eq. 3. One can express the fraction of the delocalized states as a sum of two bits $k\alpha^{z+1}$ and α^{z+2} , out of which the bigger bit loses weight at every step until it reaches α^{z+1} , where it disintegrates according to the rule defined in Eq. 3 and then the bigger bit loses weight at each step. For a specific value of α , at every step of the sequence one obtains a P_q phase.

in Eq. 3 and the new bigger bit starts losing weight at each step. This is a continuous process as depicted by the sequence in Fig. 5. For a specific choice of α , one obtains a P_q phase at each step of the sequence. The top of the sequence corresponds to the fully delocalized ($\eta = 1$) phase. One obtains P_1, P_2, \dots phases as one goes down following the sequence. The P_q phases possess DM (DL) edges if $\sigma < 1$ ($\sigma > 1$).

We show a schematic of the phase diagram in Fig. 1, where the colored regions are labelled by η in different phases. Choosing $k = 2$ in the sequence depicted in Fig. 5 leads to the phases labelled by η in Fig. 1. These phases are as follows \rightarrow red: $\eta = 2\alpha + \alpha^2 = 1$ (delocalized); green: $\eta = \alpha + \alpha^2$ (P_1); orange: $\eta = 2\alpha^2 + \alpha^3$ (P_2); purple: $\eta = \alpha^2 + \alpha^3, 2\alpha^3 + \alpha^4, \dots$ (P_3, P_4, \dots respectively) collectively, which appear as one proceeds further according to the sequence. For large values of σ and λ the localized phase appears when $\eta = 0$, shown in blue.

Entanglement entropy: Here we consider noninteracting spinless fermions in the LRH model to calculate the entanglement entropy of the fermionic ground states in different phases obtained in the previous section. The entanglement entropy in the ground state of such free fermionic systems is given by [56–58]

$$S_A = - \sum_{m=1}^L [\zeta_m \log \zeta_m + (1 - \zeta_m) \log(1 - \zeta_m)], \quad (5)$$

where ζ_m 's are the eigenvalues of the correlation matrix C^A , where $C_{ij}^A = \langle c_i^\dagger c_j \rangle$ with $i, j \in$ subsystem A

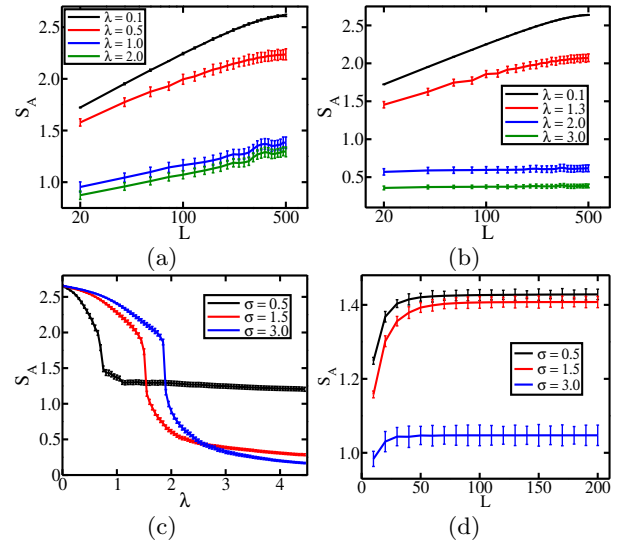


FIG. 6. (a-b) The subsystem size L dependence of entanglement entropy S_A with increasing values of λ for fermions at half-filling and for $\sigma = 0.5$ and 1.5 . (c) S_A as function of λ for $\sigma = 0.5, 1.5$ and 3.0 respectively for fermions at half-filling with $L = N/2$. For all the plots in figures (a-c) $N = 1024$. (d) Entanglement entropy S_A as a function of subsystem size L for increasing σ and fixed $\lambda = 2.2$. For all the plots $N = 512$ for α_g and special filling $\nu = \alpha_g^4$.

of L sites. For free fermions in d dimensions, typically $S_A \propto L^{d-1} \ln L$ in metallic phases [59], while it goes as $S_A \propto L^{d-1}$ in adherence to the ‘area-law’ in the localized phases in the presence of disorder.

To produce smoother plots, we employ an average of S_A over the 100 realizations of θ_p uniformly choosing from $[0, 2\pi]$ in all the plots here. We stick to filling fraction $\nu = 0.5$ of fermions unless otherwise mentioned and $\alpha_g = (\sqrt{5}-1)/2$. The S_A vs L plots are shown in Fig. 6(a) and Fig. 6(b) at half-filling with increasing values of λ for $\sigma = 0.5$ and 1.5 respectively. From Fig. 6(a) for $\sigma = 0.5$, when $\lambda = 0.1$ and 0.5 (delocalized and P_1 phases), the Fermi level is delocalized and hence $S_A \propto \ln L$. In the same figure, when $\lambda = 1.0$ and 2.0 (P_2 and P_3 phases) the Fermi level is multifractal, $S_A \propto \ln L$ but the magnitude of S_A is drastically low. In Fig. 6(b) for $\sigma = 1.5$, when $\lambda = 0.1$ and 1.3 (delocalized and P_1 phases), the Fermi level is delocalized and $S_A \propto \ln L$. However, when $\lambda = 2.0$ and 3.0 (P_2 and P_3 phases) the Fermi level is localized, the magnitude of S_A is much lower, and it abides by the area-law. Transitions of Fermi level at half-filling are shown in Fig. 6(c) for $\sigma = 0.5, 1.5$ and 3.0 respectively. For $\sigma = 0.5$, the Fermi level undergoes a DM transition at $\lambda = 0.75$. For $\sigma = 1.5$ and 3.0 the Fermi level undergoes DL transitions at $\lambda = 1.5$ and $\lambda = 1.85$ respectively, as also evident from Fig. 2(a-c).

We have also checked that the qualitative behavior of S_A vs L in the half-filled free fermionic ground state barely changes in the phase diagram for α_s and α_b . However, similar to the AAH model [45, 47], the LRH model

too shows ‘area-law’ behavior for special fillings ν even in the delocalized regime. An example of this is shown in Fig. 6(d) for $\lambda = 2.2$ and $\sigma = 0.5, 1.5, 3.0$ and special filling $\nu = \alpha_g^4$. In all these plots S_A abides by the ‘area-law’. However, the magnitude of S_A is significantly smaller for $\sigma = 3.0$. We point out that while the single particle results depend on whether the system size is a Fibonacci number, the many-particle measures do not show such a dependence on the system size (see Ref. 47 for details).

Conclusions: We uncover an intricate pattern of the localization structure of the AAH potential in the presence of long-range hoppings when the quasi-periodicity parameter is a member of the ‘metallic mean family’. In addition to the fully delocalized and localized phases we obtain a co-existence of multifractal (localized) eigenstates with delocalized eigenstates for $\sigma < 1$ ($\sigma > 1$). The fraction of delocalized eigenstates in these phases can be obtained from a general sequence which is a manifestation of a mathematical property of the ‘metallic mean family’. The entanglement entropy of a noninteracting fermionic ground state respects the area-law if the Fermi level belongs in the localized regime while logarithmically violating it if the Fermi-level belongs in the delocalized or multifractal regimes, although the magnitude in the multifractal regime is significantly lower than in the delocalized one. Entanglement entropy surprisingly follows the area-law for certain special filling fractions even in the delocalized regime. These special filling fractions are related to the metallic means. In this work, we make an attempt to show how the inherent mathematical structure in the ‘metallic means’ manifests itself in the single particle and many particle properties of a class of quasi-periodic models. Studies of this kind are very rare in the literature [60, 61]. Hopefully our work will help motivate further research in this direction.

Acknowledgments: N. R is grateful to the University Grants Commission (UGC), India for providing a PhD fellowship. A.S acknowledges financial support from SERB via the grant (File Number: CRG/2019/003447), and from DST via the DST-INSPIRE Faculty Award [DST/INSPIRE/04/2014/002461].

[1] A. Goldman and R. Kelton, *Reviews of modern physics* **65**, 213 (1993).
 [2] M. Kohmoto, B. Sutherland, and C. Tang, *Phys. Rev. B* **35**, 1020 (1987).
 [3] E. L. Albuquerque and M. G. Cottam, *Physics Reports* **376**, 225 (2003).
 [4] E. MacIá, *Reports on Progress in Physics* **69**, 397 (2005).
 [5] P. W. Anderson, *Phys. Rev.* **109**, 1492 (1958).
 [6] S. Aubry and G. André, *Ann. Israel Phys. Soc* **3**, 18 (1980).
 [7] P. G. Harper, *Proc. Phys. Soc. A* **68**, 874 (1955).
 [8] S. D. Sarma, S. He, and X. Xie, *Physical Review B* **41**, 5544 (1990).

[9] S. Ganeshan, J. Pixley, and S. D. Sarma, *Physical review letters* **114**, 146601 (2015).
 [10] Y. Lahini, R. Pugatch, F. Pozzi, M. Sorel, R. Morandotti, N. Davidson, and Y. Silberberg, *Phys. Rev. Lett.* **103**, 013901 (2009).
 [11] E. Lucioni, B. Deissler, L. Tanzi, G. Roati, M. Zaccanti, M. Modugno, M. Larcher, F. Dalfovo, M. Inguscio, and G. Modugno, *Physical review letters* **106**, 230403 (2011).
 [12] J. Lye, L. Fallani, M. Modugno, D. Wiersma, C. Fort, and M. Inguscio, *Physical review letters* **95**, 070401 (2005).
 [13] M. Schreiber, S. S. Hodgman, P. Bordia, H. P. Lüschen, M. H. Fischer, R. Vosk, E. Altman, U. Schneider, and I. Bloch, *Science* **349**, 842 (2015).
 [14] V. Oganesyan and D. A. Huse, *Physical review b* **75**, 155111 (2007).
 [15] F. Alet and N. Laflorencie, *Comptes Rendus Physique* **19**, 498 (2018), quantum simulation / Simulation quantitative.
 [16] D. A. Abanin, E. Altman, I. Bloch, and M. Serbyn, *Reviews of Modern Physics* **91**, 021001 (2019).
 [17] S. Iyer, V. Oganesyan, G. Refael, and D. A. Huse, *Phys. Rev. B* **87**, 134202 (2013).
 [18] R. Modak and S. Mukerjee, *Physical review letters* **115**, 230401 (2015).
 [19] M. Žnidarič and M. Ljubotina, *Proceedings of the National Academy of Sciences* **115**, 4595 (2018).
 [20] S. Xu, X. Li, Y.-T. Hsu, B. Swingle, and S. D. Sarma, *Physical Review Research* **1**, 032039 (2019).
 [21] N. Nesi and A. Iucci, *Physical Review A* **84**, 063614 (2011).
 [22] N. Roy and S. Sinha, *Journal of Statistical Mechanics: Theory and Experiment* **2018**, 053106 (2018).
 [23] V. Michal, B. Altshuler, and G. Shlyapnikov, *Physical review letters* **113**, 045304 (2014).
 [24] K. Kim, M.-S. Chang, S. Korenblit, R. Islam, E. E. Edwards, J. K. Freericks, G.-D. Lin, L.-M. Duan, and C. Monroe, *Nature* **465**, 590 EP (2010).
 [25] P. Richerme, Z.-X. Gong, A. Lee, C. Senko, J. Smith, M. Foss-Feig, S. Michalakakis, A. V. Gorshkov, and C. Monroe, *Nature* **511**, 198 (2014), letter.
 [26] J. W. Britton, B. C. Sawyer, A. C. Keith, C. C. J. Wang, J. K. Freericks, H. Uys, M. J. Biercuk, and J. J. Bollinger, *Nature* **484**, 489 EP (2012).
 [27] R. Islam, C. Senko, W. C. Campbell, S. Korenblit, J. Smith, A. Lee, E. E. Edwards, C.-C. J. Wang, J. K. Freericks, and C. Monroe, *Science* **340**, 583 (2013).
 [28] R. Islam, C. Senko, W. C. Campbell, S. Korenblit, J. Smith, A. Lee, E. E. Edwards, C.-C. J. Wang, J. K. Freericks, and C. Monroe, *Science* **340**, 583 (2013).
 [29] R. Löw, H. Weimer, U. Krohn, R. Heidemann, V. Bendkowsky, B. Butscher, H. P. Büchler, and T. Pfau, *Phys. Rev. A* **80**, 033422 (2009).
 [30] H. Weimer, R. Löw, T. Pfau, and H. P. Büchler, *Phys. Rev. Lett.* **101**, 250601 (2008).
 [31] H. Labuhn, D. Barredo, S. Ravets, S. de Léséleuc, T. Macrì, T. Lahaye, and A. Browaeys, *Nature* **534**, 667 EP (2016).
 [32] P. Schauß, J. Zeiher, T. Fukuhara, S. Hild, M. Cheneau, T. Macrì, T. Pohl, I. Bloch, and C. Gross, *Science* **347**, 1455 (2015).
 [33] S. Baier, D. Petter, J. Becher, A. Patscheider, G. Natale, L. Chomaz, M. Mark, and F. Ferlaino, *Physical review letters* **121**, 093602 (2018).

- [34] A. V. Gorshkov, S. R. Manmana, G. Chen, E. Demler, M. D. Lukin, and A. M. Rey, *Phys. Rev. A* **84**, 033619 (2011).
- [35] S. R. Manmana, E. M. Stoudenmire, K. R. A. Hazzard, A. M. Rey, and A. V. Gorshkov, *Phys. Rev. B* **87**, 081106 (2013).
- [36] B. Yan, S. A. Moses, B. Gadway, J. P. Covey, K. R. A. Hazzard, A. M. Rey, D. S. Jin, and J. Ye, *Nature* **501**, 521 EP (2013).
- [37] N. Roy, A. Sharma, and R. Mukherjee, *Phys. Rev. A* **99**, 052342 (2019).
- [38] R. P. A. Lima, H. R. da Cruz, J. C. Cressoni, and M. L. Lyra, *Phys. Rev. B* **69**, 165117 (2004).
- [39] A. D. Mirlin, Y. V. Fyodorov, F.-M. Dittes, J. Quezada, and T. H. Seligman, *Phys. Rev. E* **54**, 3221 (1996).
- [40] G. Celardo, R. Kaiser, and F. Borgonovi, *Physical Review B* **94**, 144206 (2016).
- [41] X. Deng, V. E. Kravtsov, G. V. Shlyapnikov, and L. Santos, *Phys. Rev. Lett.* **120**, 110602 (2018).
- [42] X. Deng, S. Ray, S. Sinha, G. Shlyapnikov, and L. Santos, *Physical review letters* **123**, 025301 (2019).
- [43] J. Eisert, M. Cramer, and M. B. Plenio, *Rev. Mod. Phys.* **82**, 277 (2010).
- [44] N. Laflorencie, *Physics Reports* **646**, 1 (2016).
- [45] N. Roy and A. Sharma, *Physical Review B* **100**, 195143 (2019).
- [46] M. Modugno, *New Journal of Physics* **11**, 033023 (2009).
- [47] Supplementary material.
- [48] H. Cohn, *The American Mathematical Monthly* **113**, 57 (2006), <https://doi.org/10.1080/00029890.2006.11920278>.
- [49] Y. Bugeaud, *Mathematische Annalen* **341**, 677 (2008).
- [50] J. d. J. H. Serda, *arXiv preprint arXiv:1506.00144* (2015).
- [51] S. Falcon, *Applied Mathematics* **5**, 2226 (2014).
- [52] A. Chhabra and R. V. Jensen, *Phys. Rev. Lett.* **62**, 1327 (1989).
- [53] M. Janssen, *Int. J. Mod. Phys. B* **8** (1994), 10.1142/S021797929400049X.
- [54] B. Huckestein, *Rev. Mod. Phys.* **67**, 357 (1995).
- [55] E. Cuevas, *Phys. Rev. B* **68**, 184206 (2003).
- [56] I. Peschel, *Journal of Physics A: Mathematical and General* **36**, L205 (2003).
- [57] I. Peschel and V. Eisler, *Journal of Physics A: Mathematical and Theoretical* **42**, 504003 (2009).
- [58] I. Peschel, *Brazilian Journal of Physics* **42**, 267 (2012).
- [59] B. Swingle, *Phys. Rev. Lett.* **105**, 050502 (2010).
- [60] S. Thiem, M. Schreiber, and U. Grimm, *Physical Review B* **80**, 214203 (2009).
- [61] S. Thiem and M. Schreiber, *The European Physical Journal B* **83**, 415 (2011).
- [62] S. Y. Jitomirskaya, *Ann. of Math.* **150**, 1159 (1999).
- [63] S. E. Skipetrov and A. Sinha, *Phys. Rev. B* **97**, 104202 (2018).
- [64] N. Roy and A. Sharma, *Phys. Rev. B* **97**, 125116 (2018).

Supplementary Material for “Prescription for the fraction of delocalized eigenstates in the long-range AAH model”

Nilanjan Roy and Auditya Sharma

Department of Physics, Indian Institute of Science Education and Research, Bhopal, Madhya Pradesh 462066, India

The supplementary material is divided into two sections. First we discuss the results involving the inverse participation ratio (IPR), fractal dimension and entanglement entropy of the AAH model with nearest-neighbor hopping ($\sigma \rightarrow \infty$ limit of the LRH model) and quasi-periodic potential. Next we calculate the IPR and multifractality of the eigenstates in the LRH model which acts as a complementary study to the main article.

IPR, FRACTAL DIMENSION AND ENTANGLEMENT ENTROPY IN THE AAH MODEL

The AAH model has a self-dual point at $\lambda = 2$, where the Hamiltonian in position space maps to itself in momentum space. As a consequence all the single-particle eigenstates are delocalized for $\lambda < 2$ and localized for $\lambda > 2$ [6, 62]. But earlier studies [45, 63] of the same model based on the ‘golden mean’ quasiperiodicity parameter have shown the existence of energy-dependent localization properties. Here we extend the study to the case of ‘metallic means’. We discuss the results for various quantities ahead.

IPR : The inverse participation ratio (IPR) is a key quantity for studying delocalization-localization transitions. It is defined as

$$I_n = \sum_{i=1}^N |\psi_n(i)|^4, \quad (6)$$

where the n^{th} normalized single particle eigenstate $|\psi_n\rangle = \sum_{i=1}^N \psi_n(i) |i\rangle$ is written in terms of the Wannier basis $|i\rangle$,

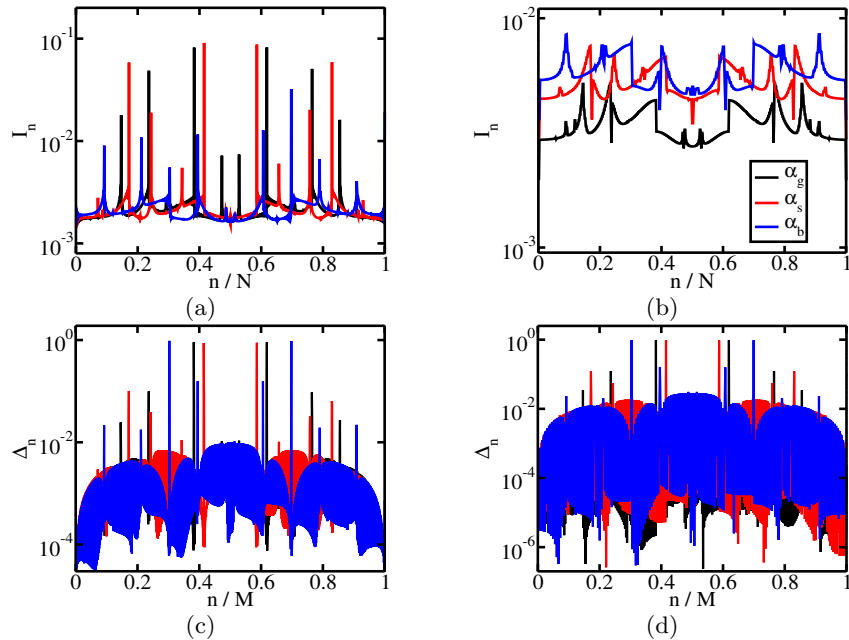


FIG. 7. (a) IPR of the single particle eigenstates I_n for different values of α and fixed $N = 1024$. (b) Similar plots for $N = 610, 408$ and 360 for α_g, α_s and α_b respectively. For these plots n/N in the x-axis stands for the fractional index of eigenstates. (c) Consecutive level-spacings $\Delta_n = E_{n+1} - E_n$ for different values of α and fixed $N = 1024$. (d) Δ_n 's for $N = 610, 408$ and 360 for α_g, α_s and α_b respectively. n/M in the x-axis stands for the fractional index of level-spacings, where total number of spacings $M = N - 1$. For all the plots $\lambda = 1$ in the AAH model. The legend shown in figure (b) applies also to figures (a), (c) and (d).

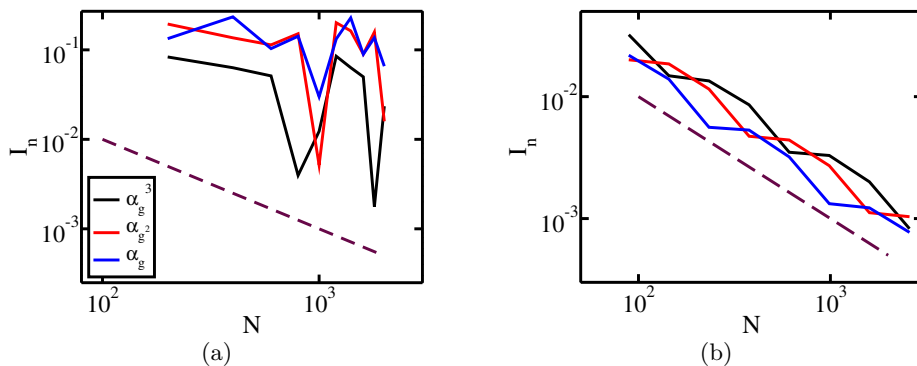


FIG. 8. (a) IPR of the special eigenstates with fractional index $n/N = \alpha_g^3, \alpha_g^2, \alpha_g$ as a function of system size N , which is a non-Fibonacci number. (b) Similar plots for N , which is a Fibonacci number corresponding to α_g . For all the plots $\lambda = 1$. The dashed line represents $1/N$ dependence of IPR of the non-special delocalized eigenstates.

representing the state of a single particle localized at the site i of the lattice. For a delocalized eigenstate $I_n \propto N^{-1}$ whereas for a localized eigenstate $I_n \propto N^0$. For a critical state I_n shows intermediate behavior. IPR of all the single particle eigenstates for $\lambda = 1$ (delocalized phase) is shown in Fig. 7(a) for a non-Fibonacci $N = 1024$ and different values of α . There exist eigenstates with high IPR for fractional index $n/N = \alpha_g, \alpha_g^2, \alpha_g^3$ ($\approx 0.618, 0.382, 0.236$) etc. for the ‘golden mean’. Similarly high- IPR eigenstates are also found for the cases of ‘silver mean’ (α_s) and ‘bronze mean’ (α_b) at $n/N = \alpha_s + \alpha_s^2, \alpha_s, \alpha_s^2 + \alpha_s^3, \alpha_s^2, \dots$ ($\approx 0.58, 0.41, 0.24, 0.17, \dots$) etc. and $n/N = 2\alpha_b + \alpha_b^2, \alpha_b + \alpha_b^2, \alpha_b, \dots$ ($\approx 0.69, 0.39, 0.3, \dots$) respectively. The single-particle energy spectra of these systems show large gaps at the positions where the high- IPR states exist [45] as shown in Fig. 7(c). In this figure the level-spacing $\Delta_n = E_{n+1} - E_n$ with E_n being the energy of the n^{th} eigenstate. Total number of level-spacings $M = N - 1$.

These high- IPR eigenstates seem to vanish if N is chosen to be a Fibonacci number as shown in Fig. 7(b) for $\lambda = 1$ and $N = 610, 360$ and 408 for α_g, α_s and α_b respectively. However, we remark that the large gaps still continue to persist in the energy spectra as also shown in Fig. 7(d). The high- IPR eigenstates show an anomalous system size dependence. As an example we show the scaling of IPR of the special eigenstates with N in Fig. 8 for $\lambda = 1.0$ and α_g . Here N is restricted respectively to be non-Fibonacci and Fibonacci in Fig. 8(a) and (b). For non-Fibonacci N the scaling behavior is severely anomalous and deviates from $1/N$. For Fibonacci N the scaling behavior is less anomalous and close to $1/N$ although not exactly $1/N$ which is represented by the dashed line for non-special delocalized eigenstates.

Fractal dimension: The fractal dimension D_2 is calculated for each single particle eigenstate for $\lambda = 1$ and different parameters α_g, α_s and α_b in a system of non-Fibonacci number of sites $N = 1000$ as shown in Fig. 9(a). In the

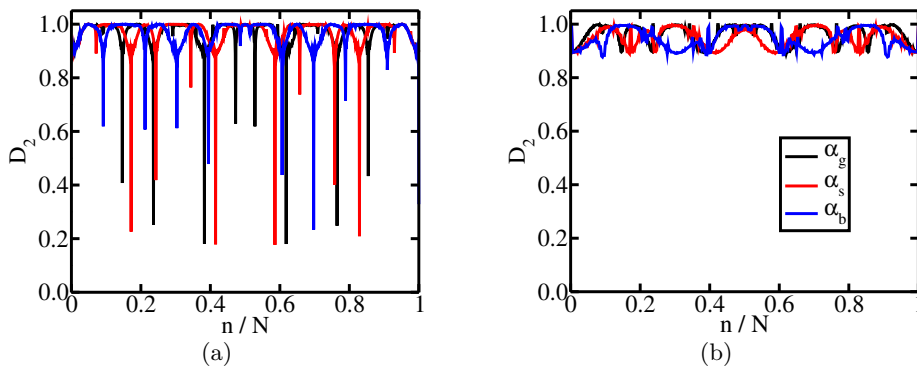


FIG. 9. (a) Fractal dimension D_2 of the single particle eigenstates for different values of α and fixed $N = 1000$. (b) Similar plots for $N = 610, 408$ and 360 for α_g, α_s and α_b respectively. For all the plots $\lambda = 1$ in the AAH model. n/N in the x-axis stands for fractional index. Here $\delta = 1/N_l = 0.01$.

delocalized phase $D_2 \approx 1$ for the majority of the eigenstates. The large deviations from $D_2 \approx 1$ are observed at the fractional eigenstate index $n/N \approx \alpha_g, \alpha_g^2, \alpha_g^3$ etc. for α_g . Similar deviations can be seen at $n/N \approx \alpha_s + \alpha_s^2, \alpha_s, \alpha_s^2 + \alpha_s^3, \alpha_s^2$ etc. for α_s , and $n/N \approx 2\alpha_b + \alpha_b^2, \alpha_b + \alpha_b^2, \alpha_b$ etc. for α_b . For these special eigenstates $0 < D_2 < 1$ which implies the presence of non-delocalized states. Fig. 9(b) indicates that the large fluctuations of D_2 vanish and $D_2 \approx 1$ for all the eigenstates when a Fibonacci number is chosen for N .

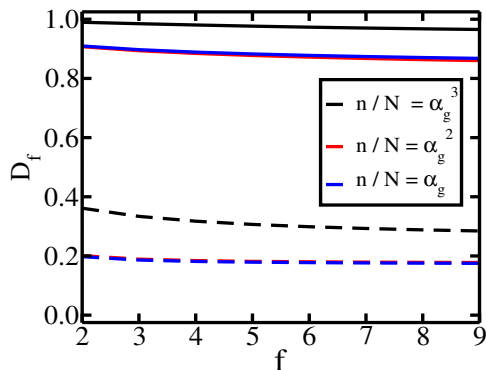


FIG. 10. Fractal dimension D_f as a function of f for the single particle eigenstates with fractional index $n/N = \alpha_g^3, \alpha_g^2, \alpha_g$. The solid lines represent plots for Fibonacci $N = 610$ whereas the dashed lines represent plots for non-Fibonacci $N = 1000$. For all the plots, $\lambda = 1$, $\alpha = \alpha_g$ and $\delta = 1/N_l = 0.01$.

In Fig. 10 we show the fractal dimension D_f as a function of f for the eigenstates with fractional index $n/N = \alpha_g^3, \alpha_g^2, \alpha_g$ for $\lambda = 1$ and ‘golden mean’ α_g . In this figure the solid lines represent the plots for Fibonacci $N = 610$ whereas the dashed lines represent the plots for non-Fibonacci $N = 1000$. We observe that the solid lines change very little with f and are close to 1. Here D_f deviates a little from 1 because these eigenstates are not perfectly delocalized as depicted in Fig. 8(b). On the other hand the dashed lines show a small variation with f and their typical value is just a fraction of one. This indicates that for non-Fibonacci N , the special eigenstates with high IPR are weakly multifractal whereas for Fibonacci N , the special eigenstates become (almost) delocalized like all the non-special eigenstates in the system. This is true even for ‘silver mean’ α_s and ‘bronze mean’ α_b (not shown here).

Entanglement entropy: The ground state entanglement entropy S_A of half the system (subsystem $L = N/2$) as a function of filling fraction ν for $\lambda = 1$ is shown in Fig. 11(a) for a non-Fibonacci $N = 256$ and different values of α . Here $\nu = N_p/N$ where N_p and N are the number of particles and number of sites respectively. Similar to high IPR in Fig. 7(a), significantly low S_A is found at $\nu \approx \alpha_g, \alpha_g^2, \alpha_g^3$ etc. for α_g ; $\nu \approx \alpha_s + \alpha_s^2, \alpha_s, \alpha_s^2 + \alpha_s^3, \alpha_s^2$ etc. for α_s ; $\nu \approx \alpha_b + \alpha_b^2, \alpha_b + \alpha_b^2, \alpha_b$ etc. for α_b . But in contrast to Fig. 7(b) of IPR , the low S_A regions seem to persist as shown in Fig. 11(b) even for Fibonacci $N = 610, 408, 360$ for $\alpha_g, \alpha_s, \alpha_b$ respectively. In the delocalized phase, $S_A \propto \ln L$ [45] for all values of ν except for the special values of ν where S_A abides by the ‘area law’ with significantly smaller magnitudes. The signature of criticality in the model is absent for special ν . These properties of the special ν have been shown earlier in Ref. 45 for α_g and hold good for α_s and α_b also. However, the non-special half-filled ($\nu = 0.5$) ground state shows $S_A \propto \ln L$ both in the delocalized phase and at the critical point (almost $\ln L$) whereas $S_A \propto L^0$ in the localized phase [64]. Although the value of S_A at the critical point is larger than that in the localized phase, it is smaller than that in the delocalized phase.

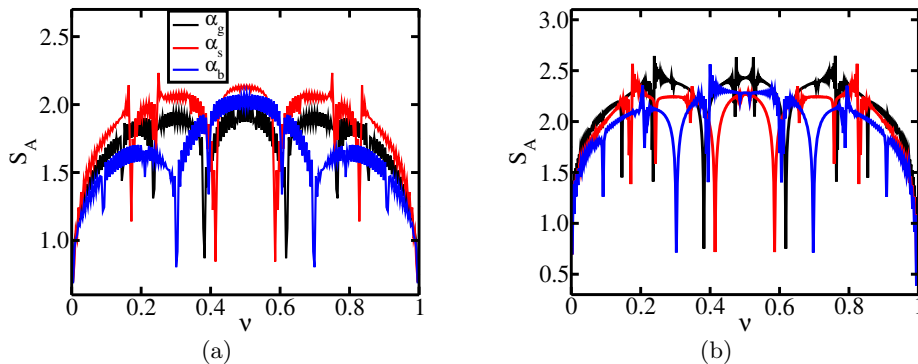


FIG. 11. (a) Entanglement entropy S_A of the ground state as a function of fermionic filling ν for different values of α and fixed $N = 256$. (b) Similar plots for $N = 610, 408$ and 360 for α_g, α_s and α_b respectively. For all the plots $\lambda = 1$ in the AAH model and size of subsystem A is $L = N/2$.

IPR AND FRACTAL DIMENSION IN THE LRH MODEL

Here we calculate IPR of the eigenstates for the LRH model with finite σ . To get a hint about the phases in the model, here we choose a fixed $\lambda = 2.2$ (which corresponds to the localized phase in the $\sigma \rightarrow \infty$ limit) and different values of $\sigma = 0.5, 1.5, 3.0$ for quasi-periodicity parameters α_g, α_s and α_b . The IPR of all the single particle eigenstates for α_g are shown in Fig. 12(a),(b) and (c) for $\sigma = 0.5, 1.5$ and 3.0 respectively. Fig. 12(a) shows that the eigenstates

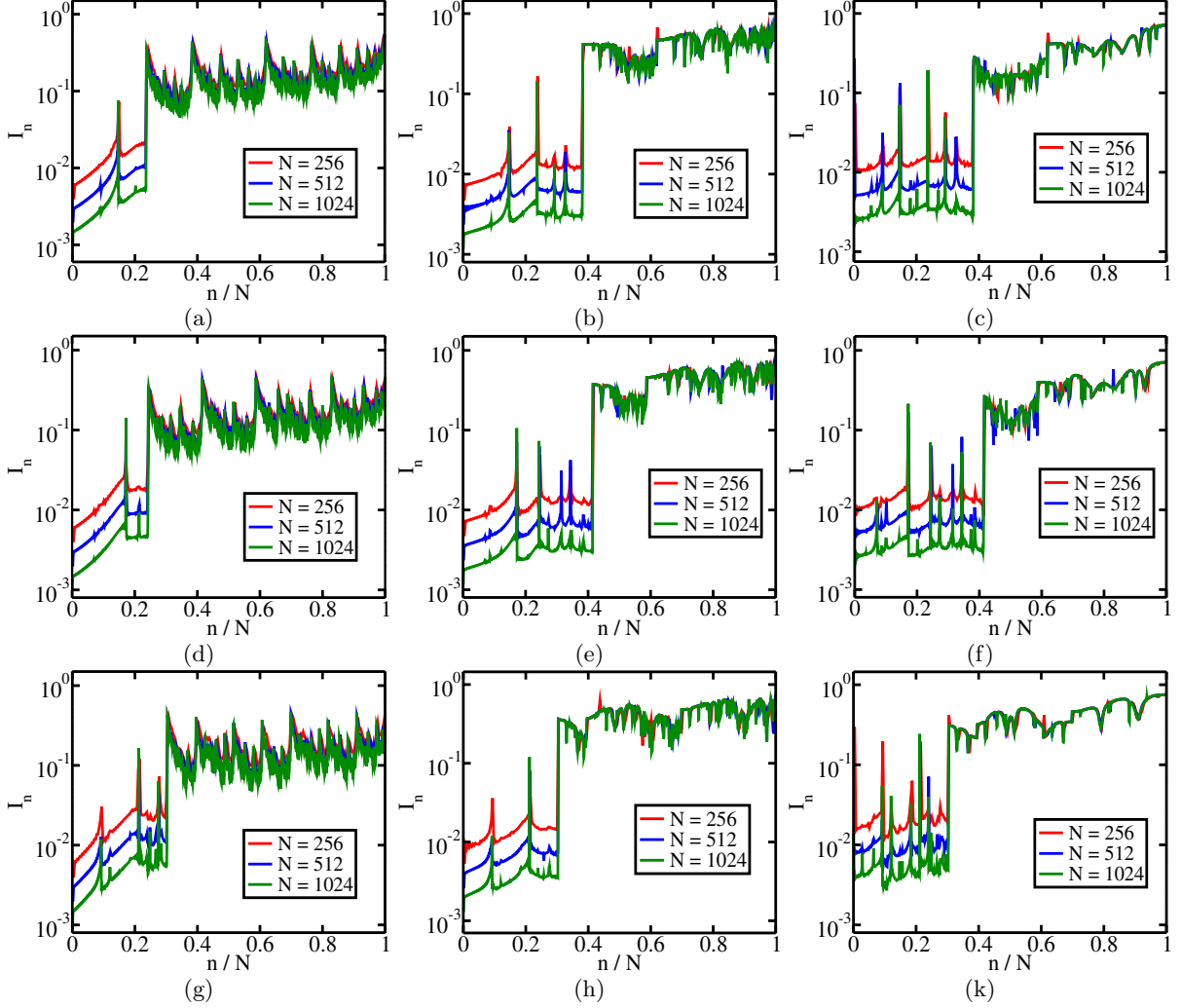


FIG. 12. (a-c) The inverse participation ratio I_n of the single-particle eigenstates for $\alpha_g = (\sqrt{5} - 1)/2$ with increasing system sizes $N = 256, 512, 1024$ for $\sigma = 0.5, 1.5$ and 3.0 respectively. (d-f) Similar plots for $\alpha_s = (\sqrt{2} - 1)$ with increasing N for $\sigma = 0.5, 1.5$ and 3.0 respectively. (h-k) Similar plots for $\alpha_b = (\sqrt{13} - 3)/2$ with increasing N for $\sigma = 0.5, 1.5$ and 3.0 respectively. For all the plots, λ is kept fixed at $\lambda = 2.2$. n/N is the fractional eigenstate index.

are delocalized ($I_n \propto N^{-1}$) as long as the fractional index $n/N < \alpha_g^3$. The IPR of the remaining eigenstates for $n/N > \alpha_g^3$ shows an intermediate dependence on N i.e. $N^{-1} < I_n < N^0$. It turns out that these eigenstates are multifractal [42](see Fig. 13(a)). Hence a DM edge exists at $n/N = \alpha_g^3$ for $\sigma = 0.5$ and $\lambda = 2.2$. As shown in Fig. 12(b) and Fig. 12(c) the eigenstates are delocalized for $n/N < \alpha_g^2$ whereas the eigenstates are localized ($I_n \propto N^0$) for $n/N > \alpha_g^2$ for the same λ and $\sigma = 1.5$ and 3.0 respectively. This implies that there exists a DL (mobility) edge for $\lambda = 2.2$ and $\sigma = 1.5, 3.0$. Also we notice that the fraction of the delocalized eigenstates can change with σ for a fixed λ . However, the occasional fluctuations of IPR as discussed for the AAH model, especially in the delocalized regimes are also visible for the LRH model, since values of N are chosen to be non-Fibonacci numbers in all the plots of Fig. 12.

We also show the results obtained from the LRH model for the silver and bronze means. Plots obtained using α_s and $\lambda = 2.2$ are shown in Fig 12(d-f) for $\sigma = 0.5, 1.5$ and 3.0 respectively. These figures indicate that there is a DM

edge at $n/N \approx \alpha_s^2 + \alpha_s^3$ for $\sigma = 0.5$ whereas there is a DL edge at $n/N \approx \alpha_s$ for $\sigma = 1.5$ and 3.0 . Fig. 12(g-k) are obtained using fixed α_b , $\lambda = 2.2$ for $\sigma = 0.5, 1.5$ and 3.0 respectively. It can be seen from Fig. 12(g-k) that there is a DM edge at $n/N \approx \alpha_b$ for $\sigma = 0.5$ whereas a DL edge exists at $n/N \approx \alpha_b$ for $\sigma = 1.5$ and 3.0 . We see that in every plot of Fig. 12 the fraction of delocalized eigenstates can always be expressed as a function of the parameter α . However, the *IPR* fluctuations in the delocalized regime continue to persist in these cases also, although they vanish if N is a Fibonacci number. It is noticeable that the *IPR* fluctuations increase in the delocalized regime with σ .

Fractal dimension: As evidence for multifractality we plot $\langle D_f \rangle$ as a function of f for the P_2 phase (with α_g^2 fraction of delocalized states) for $\sigma = 0.5$ (in Fig. 13(a)) and $\sigma = 1.5$ (in Fig. 13(b)) in the LRH model with the ‘golden mean’ α_g . Here $\langle D_f \rangle$ denotes D_f averaged over α_g^2 fraction of delocalized and $(1 - \alpha_g^2)$ fraction of non-delocalized eigenstates. We chose a Fibonacci system size $N = 987$ to avoid fluctuations due to high-*IPR* eigenstates in the delocalized phase. In Fig. 13(a) and Fig. 13(b) $\langle D_f \rangle$ averaged over α_g^2 fraction of eigenstates shows a similar small variation with f with $\langle D_f \rangle$ being close to 1, which implies these states are delocalized. $\langle D_f \rangle$ averaged over $(1 - \alpha_g^2)$ fraction of eigenstates is a fraction and shows a non-trivial dependence on f for $\sigma = 0.5$ whereas $\langle D_f \rangle$ is close to 0 and shows almost no dependence on f for $\sigma = 1.5$. This indicates that these states are multifractal for $\sigma = 0.5$ and localized for $\sigma = 1.5$. Similar states can be found in the other P_q phases corresponding to α_s and α_b .

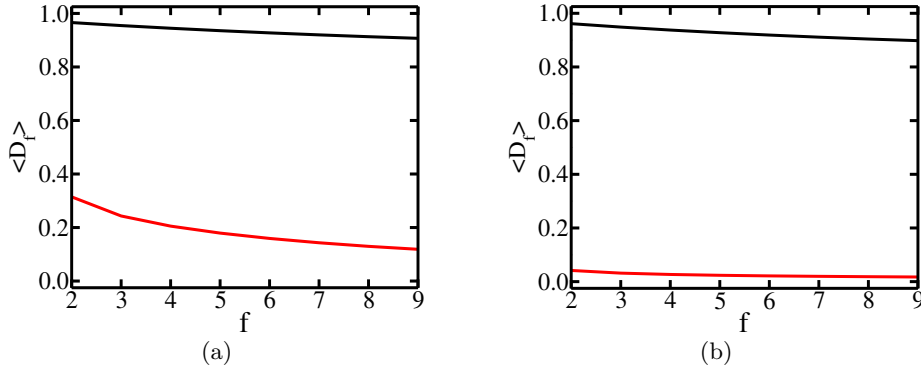


FIG. 13. (a) Averaged $\langle D_f \rangle$ as a function of f for $\lambda = 1.0$ and $\sigma = 0.5$ for which the system is in the P_2 phase with a DM edge. (b) Similar plots for $\lambda = 2.0$ and $\sigma = 1.5$ for which the system is in the P_2 phase with a DL edge. $\langle D_f \rangle$ is calculated by averaging over α_g^2 fraction of delocalized and $(1 - \alpha_g^2)$ fraction of multifractal/localized eigenstates. For all the plots system size $N = 987$ and $\delta = 1/N_l = 0.02$.